Eurographics Symposium on Rendering (2026)
I. Gkioulekas and A. Jarabo (Editors)

Differentiable Radiosity for Inverse Rendering — Supplementary Material

Appendix A: Blinn-Phong material parameters derivatives

In this section, we derive the material parameters derivatives for the Blinn-Phong model, used in our implementation. The coefficient of the matrix $\mathbf{K}$ related to a triangle k and bins i and o is:

$$\mathbf{K}(Bk+i, Bk+o) = f_k(-\omega_i, \omega_o) s_k a_k \langle \omega_o, n_k \rangle . \tag{1}$$

For this triangle k, the Blinn-Phong BRDF can be described in our case by:

$$f_k(-\omega_i, \omega_o) = \delta_k \frac{\rho_k}{\pi} \langle -\omega_i, n_k \rangle + \sigma_k \frac{p_k+2}{2\pi} \langle h(-\omega_i, \omega_o), n_k \rangle^{p_k} , \tag{2}$$

where $\theta_k = (\delta_k, \rho_k, \sigma_k, p_k)$ are the material parameters (respectively the diffuse reflection constant, albedo, specular reflection constant, and specular power), and $h(-\omega_i, \omega_o)$ the normalized half-vector. Then we can compute the derivatives of the reflection operator:

$$\frac{\partial \mathbf{K}}{\partial \theta_k} = \frac{\partial f_k}{\partial \theta_k}(-\omega_i, \omega_o)\, s_i a_k \langle \omega_o, n_k \rangle , \tag{3}$$

with:

$$\begin{aligned}
\frac{\partial f_k}{\partial \delta_k}(-\omega_i, \omega_o) &= \frac{\rho_k}{\pi} \langle -\omega_i, n_k \rangle \\
\frac{\partial f_k}{\partial \rho_k}(-\omega_i, \omega_o) &= \delta_k \frac{1}{\pi} \langle -\omega_i, n_k \rangle \\
\frac{\partial f_k}{\partial \sigma_k}(-\omega_i, \omega_o) &= \frac{p_k+2}{2\pi} \langle h(-\omega_i, \omega_o), n_k \rangle^{p_k} \\
\frac{\partial f_k}{\partial p_k}(-\omega_i, \omega_o) &= \frac{\sigma_k}{2\pi} (1 + (p_k+2) \log(\langle h(-\omega_i, \omega_o), n_k \rangle)) \\
&\quad \langle h(-\omega_i, \omega_o), n_k \rangle^{p_k}
\end{aligned}$$

Appendix B: Transport and sampling operators derivatives with respect to positions

In this section, we provide the derivatives of the transport operator $\mathbf{U}$ and $\mathcal{S}$ w.r.t. the position tensor P. As it is needed in both cases, we begin by giving the definition and derivatives of the interpolation operator $T(\omega)$. The bilinear interpolation is done using spherical coordinates (θ, ϕ) of the normalized direction ω. The four bins closest to ω are noted b, b_θ, b_ϕ, and $b_{\phi\theta}$, as illustrated next to this paragraph. If we note f the radiance distribution being interpolated, and $(\Delta\theta, \Delta\phi)$ the angular discretization steps, the interpolated value is then:

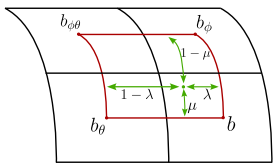

$$\begin{aligned}
&(1-\lambda)(1-\mu) f(b) + \lambda(1-\mu) f(b_\theta) + (1-\lambda)\mu f(b_\phi) + \lambda\mu f(b_{\phi\lambda}) \\
&=: \alpha f(b) + \alpha_\lambda f(b_\lambda) + \alpha_\mu f(b_\phi) + \alpha_{\phi\lambda} f(b_{\phi\lambda})
\end{aligned}$$

where (λ, μ) are the interpolation coefficients, defined by:

$$\lambda = \left| \left\{ \frac{\phi}{\Delta\phi} \right\} - 0.5 \right| , \; \mu = \left| \left\{ \frac{\theta}{\Delta\theta} \right\} - 0.5 \right| \tag{4}$$

with $\{\cdot\}$ the fractional part. Differentiating the interpolation operator boils down to differentiating λ and μ. As $(\theta, \phi) = (\text{atan2}(\omega.y, \omega.x), \text{acos}(\omega.z))$, we have:

$$\frac{\partial \lambda}{\partial \omega} = \text{sgn}\left(\left\{ \frac{\phi}{\Delta\phi} \right\} - 0.5 \right) \frac{1}{\Delta\phi} \begin{bmatrix} 0 \\ 0 \\ -\frac{1}{\sqrt{1-\omega.z^2}} \end{bmatrix}^\top$$

$$\frac{\partial \mu}{\partial \omega} = \text{sgn}\left(\left\{ \frac{\theta}{\Delta\theta} \right\} - 0.5 \right) \frac{1}{\Delta\theta} \begin{bmatrix} -\frac{\omega.y}{\omega.x^2+\omega.y^2} \\ \frac{\omega.x}{\omega.x^2+\omega.y^2} \\ 0 \end{bmatrix}^\top$$

We will also need the derivative of $x_{ji}^{(s)}$, the normalized direction from triangle i to j expressed in a frame local to the source triangle i, with respect to both positions x_i and x_j. We can write $x_{ji}^{(s)} = R_i \frac{x_j - x_i}{||x_j - x_i||}$ where R_i is the rotation matrix to a frame local to triangle i. Using the definition, we can compute:

$$\begin{aligned}
\frac{\partial x_{ji}^{(s)}}{\partial x_i} &= \frac{1}{||x_j - x_i||} \left(x_{ji}^{(s)} x_{ji}^\top - R_i \right) \\
\frac{\partial x_{ji}^{(s)}}{\partial x_j} &= \frac{1}{||x_j - x_i||} \left(-x_{ji}^{(s)} x_{ji}^\top + R_i \right) .
\end{aligned} \tag{5}$$

and similarly for $x_{ji}^{(d)} = R_j \frac{x_j - x_i}{||x_j - x_i||}$.

Finally, we can compute the derivatives for the sampling and interpolation operators. We will first go trough the sampling operator.

We recall that, for a triangle i and camera center c:

$$\mathcal{S}(i,c) = \max\left(\frac{1}{x_{ci}^{(s)}.z}, 0\right)\frac{1}{a_i}T\left(x_{ci}^{(s)}\right).$$

So we have:

$$\begin{aligned}\frac{\partial \mathcal{S}}{\partial x_i}(i,c) = &-\delta_{\geq 0}\left(x_{ci}^{(s)}.z\right)\frac{\partial\left(x_{ci}^{(s)}.z\right)}{\partial x_i}\frac{1}{\left(x_{ci}^{(s)}.z\right)^2\cdot a_i}T\left(x_{ci}^{(s)}\right)^\top \\ &+\max\left(\frac{1}{x_{ci}^{(s)}.z}, 0\right)\frac{1}{a_i}\frac{\partial T\left(x_{ci}^{(s)}\right)}{\partial x_{ci}^{(s)}}\frac{\partial x_{ci}^{(s)}}{\partial x_i},\end{aligned} \tag{6}$$

where all the necessary derivatives can be computed using the formulae above. Next, we recall the transport operator, for two different triangles i and j:

$$\mathbf{U}(i,j) = \frac{1}{\|x_{i_t} - x_{j_t}\|^2}\max\left(-x_{ji}^{(d)}.z, 0\right)T\left(x_{ji}^{(d)}\right)T\left(x_{ji}^{(s)}\right)^\top$$

If we note $r_{ij} = ||x_j - x_i||$, we have:

$$\begin{aligned}\frac{\partial \mathbf{U}}{\partial x_i}(i,j) = &\frac{2x_{ji}}{r_{ij}^3}\max\left(-x_{ji}^{(d)}, 0\right)T\left(x_{ji}^{(d)}\right)T\left(x_{ji}^{(s)}\right)^\top \\ &+\frac{1}{r_{ij}^2}\delta_{\geq 0}\left(-x_{ji}^{(d)}.z\right)\left(-\frac{\partial x_{ji}^{(d)}.z}{\partial x_i}\right)T\left(x_{ji}^{(d)}\right)T\left(x_{ji}^{(s)}\right)^\top \\ &+\frac{1}{r_{ij}^2}\max\left(-x_{ji}^{(d)}.z, 0\right)\frac{\partial T\left(x_{ji}^{(d)}\right)}{\partial x_i}T\left(x_{ji}^{(s)}\right)^\top \\ &+\frac{1}{r_{ij}^2}\max\left(-x_{ji}^{(d)}.z, 0\right)T\left(x_{ji}^{(d)}\right)\frac{\partial T\left(x_{ji}^{(s)}\right)}{\partial x_i}^\top \\ \frac{\partial \mathbf{U}}{\partial x_j}(i,j) = &-\frac{2x_{ji}}{r_{ij}^3}\max\left(-x_{ji}^{(d)}.z, 0\right)T\left(x_{ji}^{(d)}\right)T\left(x_{ji}^{(s)}\right)^\top \\ &+\frac{1}{r_{ij}^2}\delta_{\geq 0}\left(-x_{ji}^{(d)}.z\right)\left(-\frac{\partial x_{ji}^{(d)}.z}{\partial x_j}\right)T\left(x_{ji}^{(d)}\right)T\left(x_{ji}^{(s)}\right)^\top \\ &+\frac{1}{r_{ij}^2}\max\left(-x_{ji}^{(d)}.z, 0\right)\frac{\partial T\left(x_{ji}^{(d)}\right)}{\partial x_j}T\left(x_{ji}^{(s)}\right)^\top \\ &+\frac{1}{r_{ij}^2}\max\left(-x_{ji}^{(d)}.z, 0\right)T\left(x_{ji}^{(d)}\right)\frac{\partial T\left(x_{ji}^{(s)}\right)}{\partial x_j}^\top\end{aligned} \tag{7}$$

by computing, as for the sampling operator:

$$\frac{\partial T\left(x_{ji}^{(s)}\right)}{\partial x_i} = \frac{\partial T\left(x_{ji}^{(s)}\right)}{\partial x_{ji}^{(s)}}\frac{\partial x_{ji}^{(s)}}{\partial x_i},$$

for example, with the necessary derivatives given above.

Appendix C: Ambiguity between emissivity and first light bounce

In this section, we formalize the intuition that was given in Section 3.3. For the sake of clarity, let us restrict ourselves to the case of standard radiosity, with one radiance value per triangle. We still note $\mathbf{\Gamma}$ the system matrix. We introduce $\mathcal{V}$ the (orthogonal) projection of radiance distributions on a subset of triangles, corresponding to visible triangles. As $\mathbf{\Gamma}$ is full-rank, if we know the globally-illuminated radiance distribution C, there is only one corresponding emissivity distribution $E = \mathbf{\Gamma}C$. However, if some triangles are not visible, the problem becomes under-constrained. Indeed, if we take E^* a reference solution, the set of emissivity distributions E that, once globally illuminated, match E^* on *visible* triangles is $\mathcal{S} = \{E \in \mathbb{R}^N \,|\, \mathcal{V}\mathbf{\Gamma}^{-1}E = \mathcal{V}\mathbf{\Gamma}^{-1}E^*\}$, which is an affine space:

$$\mathcal{S} = E^* + \ker(\mathcal{V}\mathbf{\Gamma}^{-1}) = E^* + \mathbf{\Gamma}(\ker\mathcal{V}). \tag{8}$$

This last equality holds because $\mathbf{\Gamma}$ is full rank.

We are interested in distributions of non-negative radiances, which leads to defining the convex polytope $\mathcal{P}$ as:

$$\mathcal{P} = \mathcal{S} \cap (\mathbb{R}^+)^N. \tag{9}$$

For example, with this formulation, we can prove our initial observation. If we assume that light sources are not visible, i.e. $\mathcal{V}E^* = 0$, then we want to show that $RE^* \in \mathcal{P}$, *i.e.* the distribution after the first light bounce is a solution with non-negative radiance. This holds, because:

$$RE^* = E^* + (RE^* - E^*) = E^* + \mathbf{\Gamma}(-E^*), \tag{10}$$

and by hypothesis, $-E^* \in \ker\mathcal{V}$. This observation is generalizable to a higher number of bounces.

Appendix D: Boundedness of the convex polytope $\mathcal{P}$

In the previous section, we explained that the set of non-negative solutions to $\mathcal{V}\mathbf{\Gamma}^{-1}E = \mathcal{V}\mathbf{\Gamma}^{-1}E^*$ is a convex polytope. We assume that $0 < \dim(\ker\mathcal{V}) < N$, i.e. we exclude trivial cases. Using physical arguments, we can show that it is bounded, under reasonable assumptions.

Let us assume that $\mathcal{P}$ is not bounded. It is a convex polytope, so it means that we can find a non-zero radiance distribution $C \in \ker\mathcal{V}$ such that for all positive λ, $E^* + \lambda\mathbf{\Gamma}C \in \mathcal{P}$. In particular, it means that $\mathbf{\Gamma}C \geq 0$ (where the comparison is understood componentwise), because otherwise, for λ large enough, we would not have $E^* + \lambda\mathbf{\Gamma}C \geq 0$ anymore (which is necessary to be in the polytope).

So we are in a situation where $C \in \ker\mathcal{V}$ and $\mathbf{\Gamma}C \geq 0$. We recall that $\mathbf{\Gamma}C$ is the emissivity distribution that generates C once globally illuminated. But as $C \in \ker\mathcal{V}$, it means that some triangles have zero radiance, even though $\mathbf{\Gamma}C \geq 0$ (and $\mathbf{\Gamma}C \neq 0$ by assumption). This is not possible, because if all emissivities are non-negative, then the globally illuminated scene cannot contain zero radiance triangles (if we assume that the scene is connected, in the sense that there is a light path between any pair of triangles, which is usually the case).

Therefore, $\mathcal{P}$ is a bounded convex polytope.

Appendix E: Comparison with finite differences

To validate our gradients, we compare them with central finite differences. We present the relative error between finite differences for decreasing epsilons and our gradients for emissivity, albedo,

and position, on the cornellbox scene, averaged on a subset of triangles. Note that these tests do not include the rasterization step so that they only account for our computed gradients, and finite differences are entirely computed in double precision. The formula that we use for the relative error for parameter α (where α is emissivity, albedo, or position) is then:

$$e_\alpha(\varepsilon) = \frac{||fd_\alpha(\varepsilon) - \nabla_\alpha \mathcal{L}||_2}{||fd_\alpha(\varepsilon)||_2 + ||\nabla_\alpha \mathcal{L}||_2}, \text{ and } fd_\alpha(\varepsilon) = \frac{\mathcal{L}(\alpha+\varepsilon) - \mathcal{L}(\alpha-\varepsilon)}{2\varepsilon} \tag{11}$$

We obtain the results presented in Fig 1, and the curves for the three gradients present different behaviors.

First, Fig 1a illustrates the error for the emissivity gradients. We recall Equation (6) in Section 3.1 (discarding the –linear– sampling operator for the sake of simplicity):

$$C = \mathbf{\Gamma}^{-1} E\,. \tag{12}$$

So the resulting face colors are linear in the emissivity distribution. This is clearly visible on Figure 1a: the plateau for $\varepsilon > 10^{-4}$ illustrates the independence of the finite differences with respect to ε. In this phase, the relative error has a low value of 10^{-8}. For $\varepsilon < 10^{-4}$, the relative error starts to increase: the rounding error kicks in, and degrades precision.

For albedo gradients, results are presented in Figure 1b. We also observe two phases in the curve. For $\varepsilon > 10^{-3}$, the relative error decreases to very low values, with a minimum around 10^{-8}. Then, precision is degraded for smaller ε. However, face colors are no longer linear in the albedo distribution. Indeed, this parameter is used linearly in the $\mathbf{K}$ reflection operator, but $\mathbf{K}$ then goes through a matrix inversion to compute face colors. We recall the formula:

$$C = (I - (\mathbf{K} - \mathbf{J})\mathbf{U})^{-1} E, \text{ and } \nabla_A \mathcal{L} = \nabla_C \mathcal{L} \mathbf{\Gamma}^{-1} \frac{\partial \mathbf{K}}{\partial A} \mathbf{U} C\,. \tag{13}$$

Finally, gradients with respect to positions are presented in Figure 1c. Derivatives are more complex, so relative errors are higher than for emissivity or albedo. However, it decreases with ε, down to a relative error of nearly 10^{-3}. Note that the effect of the rounding error is not visible on this plot, because relative errors are higher than in previous cases.

Appendix F: Memory and time consumption

We give the memory and time consumptions of our method, on the mesh of the statue used in Figure 9. We subdivide or simplify the mesh so that the mesh resolution ranges from 10k to 200k triangles, and measure the VRAM usage and the computational time for one light bounce of our method. Results are presented in Figure 2. In this figure, we can see the two expected behaviors of our method: VRAM usage is linear in the mesh size, and time is quadratic in the mesh size. As in the original experiment of Figure 9, we used 130 bins per hemisphere. As we can see, at this resolution, our method uses approximately 1.8GB every 50k triangles.

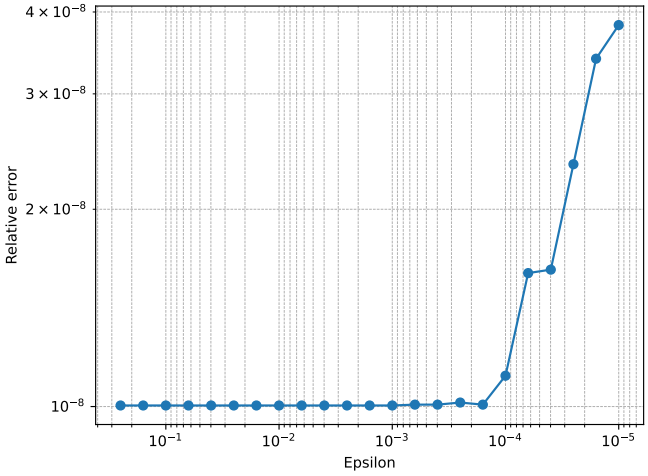

(a) Emissivity

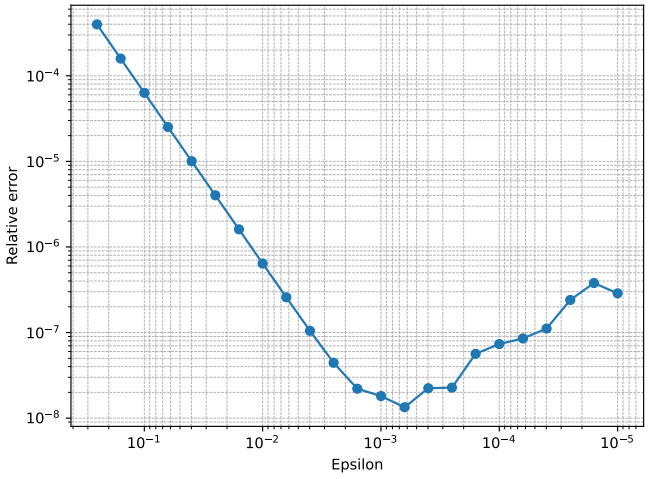

(b) Albedo

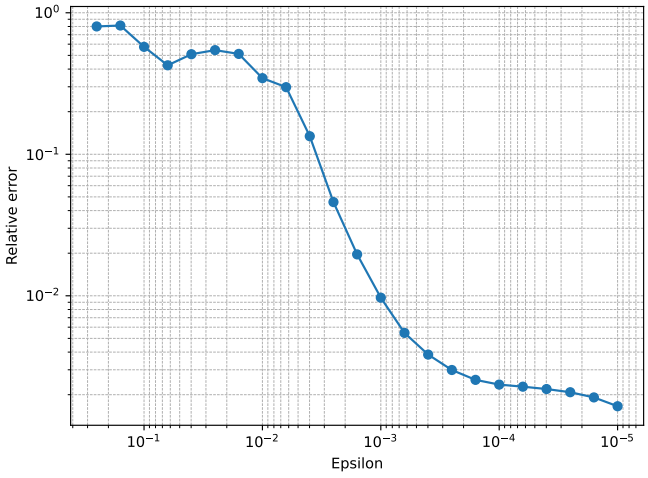

(c) Position

Figure 1: Relative error of our gradients with finite differences.

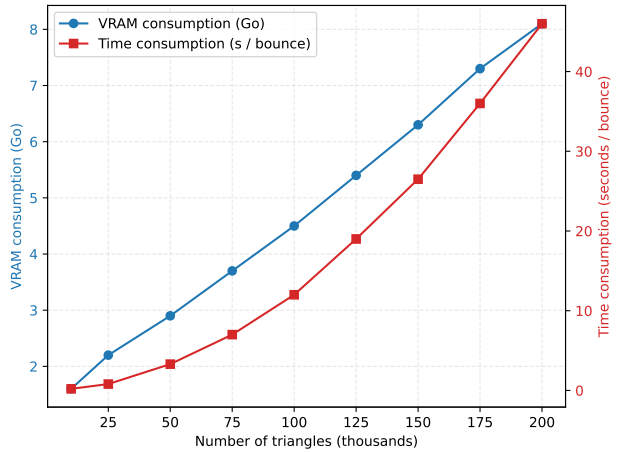

Figure 2: VRAM use and time with respect to the number of triangles.